CrossMark

Density and Refractive Index of Carbon Monoxide Ice at Different Temperatures

Ramón Luna[ID], Carlos Millán, Manuel Domingo, Carmina Santonja, and Miguel Á. Satorre
Centro de Tecnologías Físicas, Universitat Politècnica de València, Plaza Ferrándiz-Carbonell, E-03801 Alcoy, Spain; ralunam@fis.upv.es

Abstract

This paper is intended to study the density and the refractive index of the solid carbon monoxide in the interval 13–28 K to improve our understanding of the dynamics in the astrophysical environments where they are present. A series of deposition experiments have been performed under high vacuum conditions to study the properties of this ice under astrophysical conditions. Ice density has been experimentally calculated at different deposition temperatures of astrophysical interest, which complement the scarce values present in the literature. The refractive index has also been experimentally determined. The data have been used to obtain an experimental relationship between refractive index and density. Values of density are necessary to interpret observations of astrophysical objects or to design irradiation experiments to understand how irradiation affects ices present in these objects. The experimental relationship found between density and refractive index allows us to estimate density from a known refractive index, even for temperatures not reached using our experimental setup.

1. Introduction

In its solid form, carbon monoxide is one of the most abundant molecules in frozen astrophysical scenarios. It is present in a wide variety of them. This ice has been detected on the surface of some satellites such as Triton (Lellouch et al. 2010; Tegler et al. 2019), in trans-Neptunian objects (TNOs) as Pluto (Owen et al. 1993; Merlin 2015), or in the cometary nucleus (Delsemme 1983) as has been observed from the signal of the cometary tail of Hyakutake and Hale–Bopp (Hudson & Moore 1999). In the interstellar medium (ISM), this ice has been detected in the line of sight of the clouds Serpens (Chiar et al. 1994), Taurus (Whittet et al. 1989), and rho Ophiuchi (Kerr et al. 1993), in the line of sight of young stellar objects (Penteado et al. 2015), or protostars (Lacy et al. 1984).

This ubiquity is the reason to perform a plethora of studies from several areas of astronomy to disentangle the dynamics of this ice along with the corresponding solid-gas interphase. Synergies among theoretical, observational, and experimental laboratory studies are necessary to improve the knowledge on the behavior of this species in the astrophysical environment. Some of the most relevant studies on CO ice are listed below:

1. The identification of this molecule through astronomical observations was enabled by comparison to laboratory spectra of CO ice, either pure or mixed with other species that produce a shift in the absorbing feature due to their physical interactions. These laboratory studies in the infrared band have been reported by several authors (Roux et al. 1980; Ehrenfreund et al. 1996; Quirico & Schmitt 1997; Alsindi et al. 2003; Palumbo et al. 2006; Zamirri et al. 2018; Abplanalp & Kaiser 2019; Tegler et al. 2019).

2. In environments like hot cores, ices are protected from strong cosmic radiation, but they are exposed to an increasing temperature as the object evolves. Therefore, some studies are focused on thermal desorption experiments of CO. These experiments involve thermal programmed desorptions (TPD) usually in combination with the corresponding IR spectra. These works can be performed on pure CO ice (Cazaux et al. 2017), or CO mixed with other molecules (Kouchi 1990; Collings et al. 2003, 2003; Öberg et al. 2005; Bisschop et al. 2006; Acharyya et al. 2007; Martín-Doménech et al. 2014). From TPD experiments, the value of the interaction energy between molecules and the frequency factor of the Polanyi–Wigner equation can be derived (Polanyi & Wigner 1925; Luna et al. 2014).

3. In other scenarios, like in the ISM, the harsh irradiation conditions on CO act as a source for the formation of new species or changes in their structure. In the laboratory, these conditions have been reproduced to evaluate the formation of other species depending on whether pure CO is irradiated (van Dishoeck & Black 1988; Loeffler et al. 2005; Jamieson et al. 2006; Seperuelo-Duarte et al. 2010; Ciaravella et al. 2012; Huang et al. 2020; Kouchi et al. 2021) or the irradiation involves a mixture of CO along with other species: N_2, O_2, H_2O, CO_2, NH_3, CH_4, or CH_3F (Brucato et al. 1997; Hudson & Moore 1999; Satorre et al. 2000; Takano et al. 2003; Bennett et al. 2009, 2009, 2010, 2011; Kaiser et al. 2014; Maity et al. 2014; Lin et al. 2019; Schmidt et al. 2019; Turner et al. 2021). Irradiation experiments have also been used to study the photodesorption of carbon monoxide (Muñoz Caro et al. 2016). Some experimental groups use energetic hydrogen ions to irradiate CO (Schou & Pedrys 2001) instead of photon irradiation. All these works additionally need to perform IR spectra to identify the remaining species and changes in structure and composition after irradiation.

4. The surfaces of frozen astrophysical objects are generally composed of a mixture of molecules. Depending on their

relative position, the interaction between molecules, porosity, size of pores, size of molecules, etc., some molecules can diffuse through the ice matrix and eventually reach the surface. Concerning CO, some diffusion experiments are performed using the mixture of CO with CO_2 (Cooke et al. 2018) or with water (Mispelaer et al. 2013; Lauck et al. 2015; Cazaux et al. 2017; Kouchi et al. 2021) to study the energy barrier of the process.

All the CO studies exposed above have in common the need for the density parameter: concerning infrared spectroscopy (used for the first three enumerated cases), when quantification (thickness, abundance, ...) is necessary, the band strength of a feature has to be converted in the number of molecules present by means of the density through the integrated absorbance. Bouilloud et al. (2015) perform extensive work to recalculate this parameter with current values of density present in the literature (instead of assuming the previously widely used 1 g cm^{-3} for all ices and all temperatures) for CO and other molecules of astrophysical interest. Referring to irradiation experiments, laboratories need to previously plan the experiments because the irradiated ice thickness depends on the density. Concerning diffusion, the density of the ice matrix is also needed to determine the lapse of time that the diffusing molecule spends to reach the surface.

Despite the importance of the density, only scarce values have been reported so far (Roux et al. 1980; Jiang et al. 1975). Additionally, for some species, the variation of this parameter with temperature has been reported (Satorre et al. 2008, 2013, 2017). These lack of values for other temperatures relevant to astrophysical environments represent our motivation to undertake the task of determining the density and refractive index for CO deposited at different temperatures.

The present work is focused on the determination of the density and refractive index for carbon monoxide in an interval of relevant temperatures for astrophysical environments. Additionally, the Lorentz–Lorenz relationship between refractive index and density has been checked. To perform this study a series of experiments at different deposition temperatures have been carried out.

2. Experimental Setup

The deposition and desorption experiments performed in this study have been carried out in a system working under high vacuum conditions. The main components were a quartz crystal microbalance (QCMB), a double laser system (DLS), an intelligent temperature controller (ITC), and a quadrupole mass spectrometer (QMS) whose accuracy is 0.5 amu (Figure 1). The base pressure during each experiment (3×10^{-8} mbar) was obtained by assembling a pair of turbo-molecular pumps backed by their corresponding rotary pumps and the help of a closed-cycle He cryostat acting as a cryopump. The gas is deposited at a constant rate, a crucial point to obtaining refractive index and density is to use a constant flow of molecules entering the chamber. This flow is controlled by regulating two parameters: the pressure in the prechamber (measured with a capacitive sensor) and the aperture of a needle valve at the entrance. The constancy of mass rate deposition can be checked from the QCMB frequency signal, as explained below (for a more detailed explanation, see Beltrán et al. 2015).
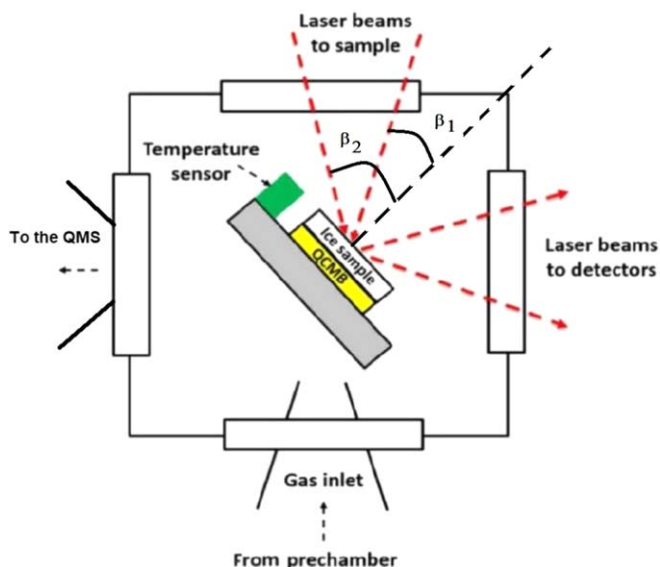

Figure 1. Main components of the experimental setup. Disposition of the laser beams and location of the QCMB, the sample, the quadrupole mass spectrometer (QMS), and one of the temperature sensors.
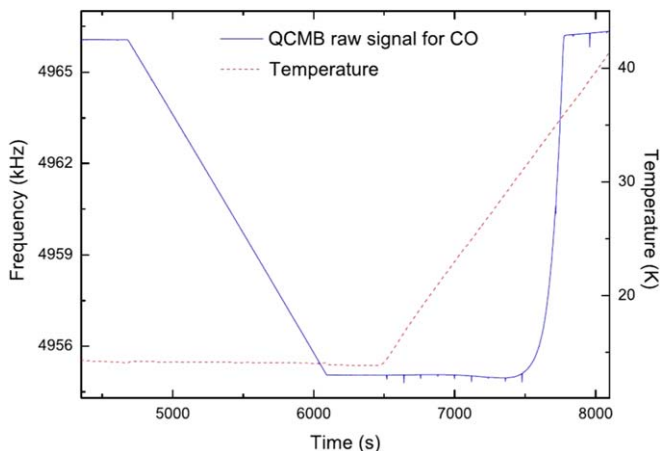
Figure 2. Frequency QCMB signal and temperature ITC signal during an experiment. The straight solid line with negative slope corresponds to the film deposition and the straight dotted line with positive slope corresponds to the desorption.

The QCMB is used as a sample holder to grow the ice during deposition. The edge of the cryostat is in thermal contact with the QCMB (gold plated quartz, $f_0 = 5$ MHz) to cool it down. The temperature of the sample (deposited onto the QCMB) is monitored by the ITC, using two silicon diode sensors, one located just beside the quartz crystal and the other one placed beside the heating resistor. The arrangement formed by the ITC and two resistors allows the temperature to be varied between 13.0 and 300.0 ± 0.1 K. The DLS (633 nm in wavelength) is used to monitor the growth of the solid film formed on the sample holder. The selected incident angles of the laser beams onto the sample are $13°5$ and $72°9$. The almost negligible variation in the QCMB frequency within the interval 4400 and 4800 s (solid line in Figure 2, just before the CO deposition starts), indicates the scarce variation in mass due to contaminants (mainly water) in our system. Extrapolating this variation to the instant 6100 s, the contaminants accreted during deposition can be estimated, leading to values of contaminants (mainly water) lower than 0.1% relative to CO. This ratio was
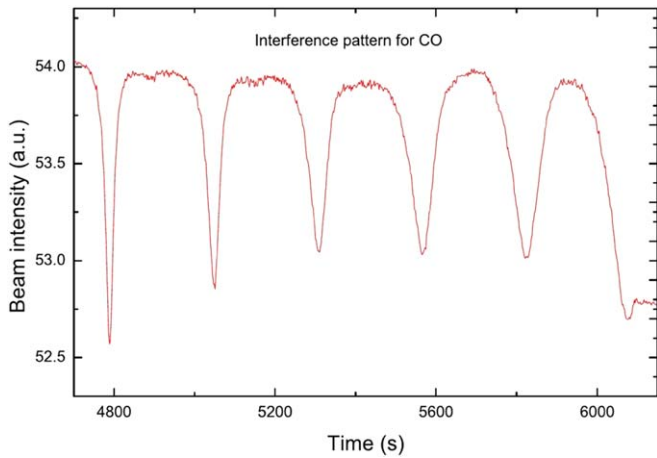
Figure 3. Interference pattern obtained from one of the He–Ne lasers during deposition of CO at 14 K. The parameter used to determine the thickness of the ice film is the distance between minimums.

also checked with the mass spectrometer from the partial pressures, confirming that water accretion can be neglected. The deposition begins when the sample holder achieves the selected temperature for each experiment. At this temperature, the gas enters the chamber and freezes on the cold substrate at a constant rate. During deposition, the pressure is maintained in the prechamber to obtain the required constant deposition rate. The pressure in the chamber during deposition is around 1×10^{-5} mbar. The signals represented in Figure 2 are acquired during one of the deposition-desorption experiments for CO. The solid line represents the collected QCMB frequency signal. The straight line with a negative slope in the interval 4800–6100 s corresponds to the deposition of the sample and its linear regression coefficient is higher than 0.9999, which validates the process (constant mass rate deposition). The film thickness obtained during these experiments is around 2–3 μm. The dotted line in this figure represents the temperature during the experiment. The desorption is performed in the interval 6500–8100 s. As can be observed, a linear positive variation in temperature has been programmed and the QCMB frequency increases when CO desorbs. Figure 3 shows the interference pattern obtained by one of the lasers of the DLS used during the growth of the CO ice for one experiment at 14 K. The change in amplitude of the fringes is associated with the instability of the laser signal and scattering. From this figure, the constancy of the deposition process can also be inferred from the constant distance (in elapsed time) between adjacent minimums. This fact also reflects that the ice structure remained unaltered during the experiment. Additionally, it is possible to observe that, at around 6100 s, when the deposition is stopped, the laser signal remains constant (as the QCMB signal does). Therefore, at this point, the film thickness does not increase anymore. This fact confirms the validity of our vacuum system to continuously remove the molecules in the chamber, maintaining an appropriate experimental base pressure.

For desorption experiments, the temperature of the sample holder is raised at a constant rate (usually 1 K min^{-1}). The QMS collects a part of the molecules released from the solid film grown on the sample holder to check the composition of the gas in the chamber during the experiment.

3. Density and Refractive Index

3.1. Determination Procedure

The density and the real part of the refractive index of ice are obtained by growing a film of the sample onto a QCMB of a known area (1.00 cm^2 for the present work). The procedure to determine these parameters is published in previous works (Satorre et al. 2013, 2017; Domingo et al. 2021). Briefly, the main steps are listed below:

The refractive index is obtained using the following expression (Wood & Roux 1982):

$$n^2 = \frac{\sin^2 \beta_{i2} - \gamma^2 \sin^2 \beta_{i1}}{1 - \gamma^2}, \quad (1)$$

where β_{i1} and β_{i2} are the angles used for the DLS, γ represents the quotient $\frac{\Delta t_1}{\Delta t_2}$, where Δt_2 (time interval between minimums) has been measured from Figure 3 at the angle β_{i2} and Δt_1 has been calculated in the same way from the signal obtained using β_{i1}.

The thickness d of the sample is usually deduced from (Roux et al. 1980; Brunetto et al. 2008):

$$d = \frac{m \, \lambda}{2 \, n \, \cos(\theta_t)}, \quad (2)$$

where m is the number of minimums used, λ is the wavelength of the incident laser, and θ_t is the angle of refraction.

The mass deposited onto the QCMB (in g cm^{-2}) comes from the Sauerbrey equation (Domingo et al. 2021):

$$\Delta m = -S\Delta f, \quad (3)$$

where Δf is the change in frequency measured from Figure 2 and S is the specific constant for each QCMB.

3.2. Data Analysis

Scarce data on density and refractive index have been reported for carbon monoxide ice so far. Roux et al. (1980) experimentally obtained a value of 0.80 g cm^{-3} and 1.27 (at 633 nm) for density and refractive index, respectively, of CO ice deposited at 20 K; Jiang et al. (1975) reported 1.03 g cm^{-3} and 1.35 (at 35 K); and Pipes et al. (1978) published a value of 1.22 for refractive index at 20 K. In the present work, the lowest value of temperature used (13 K) is due to the limit concerning the freezing capacity of our experimental system. The highest value (28 K) is the maximum temperature at which CO can be deposited in a controlled and stable manner in our vacuum chamber.

Figure 4 plots all the experimental values obtained (compiled in Table 1). The upper panel represents the results obtained for density, and the refractive index is plotted in the lower panel. In general, as can be observed, the values for density lie in the interval 0.85–0.89 g cm^{-3} and 1.28–1.30 for refractive index. Both quantities show the same profile, an initial plateau up to 19 K, a zone of instability (saw teeth shaped) between 20 and 23 K, and eventually an increase to reach a new plateau at 24 K. It is relevant obtaining the same profile for these two parameters derived from different measurements. This point reinforces that this is an actual behavior regardless of the error bars from which one could even conclude a constant value for each of these parameters. Uncertainties are obtained by statistical analysis for each temperature, using the Student's t-distribution for a 95% confidence.
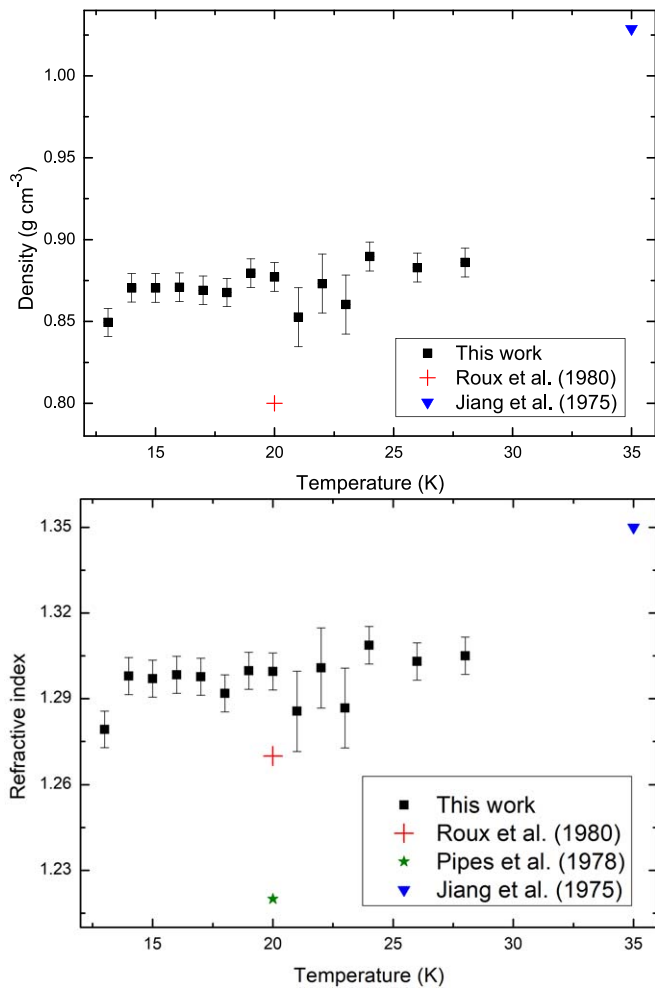
Figure 4. Average results (with error bars) for density (upper panel) and refractive index (lower panel) for CO for each temperature of deposition.

Table 1
Experimental Values for Density and Refractive Index Obtained in This Study

Temperature (K)	ρ (g cm^{-3})	n
13	0.849 ± 0.008	1.279 ± 0.006
14	0.871 ± 0.009	1.298 ± 0.006
15	0.870 ± 0.009	1.297 ± 0.006
16	0.871 ± 0.009	1.298 ± 0.006
17	0.869 ± 0.009	1.298 ± 0.006
18	0.868 ± 0.009	1.292 ± 0.006
19	0.880 ± 0.009	1.300 ± 0.006
20	0.877 ± 0.009	1.300 ± 0.006
21	0.853 ± 0.018	1.286 ± 0.014
22	0.873 ± 0.018	1.301 ± 0.014
23	0.860 ± 0.018	1.287 ± 0.014
24	0.890 ± 0.009	1.309 ± 0.007
26	0.883 ± 0.009	1.303 ± 0.007
28	0.886 ± 0.009	1.305 ± 0.007

The zone around 22 K is remarkable since a significantly larger dispersion for density and refractive index was obtained. These experiments have been repeated more times (8–10) than for the rest of the temperatures (3–5) to confirm this trend. This result could be related to a feature of the structure of CO at this temperature. This behavior is in agreement with the results obtained by Muñoz Caro et al. (2016) from the analysis of their
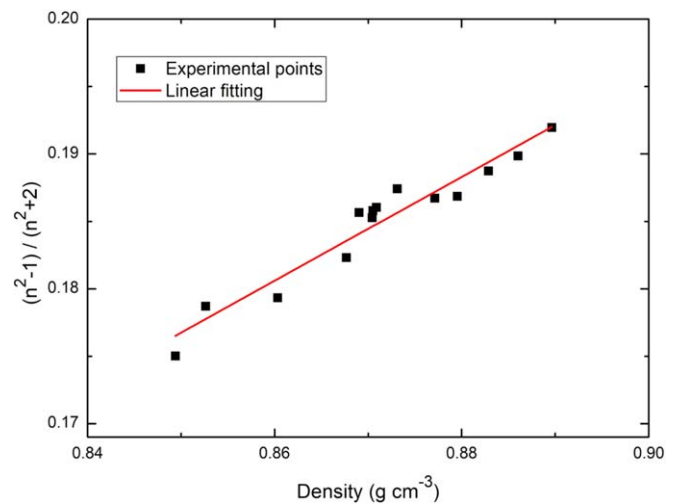
Figure 5. Experimental linear relationship of the quotient $\frac{n^2-1}{n^2+2}$ vs. density. The correlation coefficient is higher than 0.96.

infrared studies, when a change in photodesorption is detected above 20 K, Kouchi (1990) reports a shift from amorphous to crystalline at 23 K based on electron diffraction, and Lasne et al. (2015) propose at 20 K, the generation of a spontaneous field (spontelectric effect) for solid CO due to its dipole molecules.

Concerning the values reported by other authors, Roux et al. (1980) obtain similar values to those calculated in this work. Jiang et al. (1975) obtained higher values but at a significantly higher temperature (35 K) since their experimental system does not allow lower temperatures. The value reported by Pipes et al. (1978) for the refractive index at 20 K differs in ∼5% from the others.

The new results for density obtained in this work, complement the scarce previously reported values, and they are relevant to calculate band strengths to design irradiation experiments, establish limits on penetration depths, or quantify the amount of CO measured in IR astronomical observations or the IR laboratory experiments.

4. An Experimental Relationship between Density and Refractive Index: the Lorentz–Lorenz Equation

In the literature, a larger database on refractive index than on density exists since more complex laboratory experiments are involved to calculate the latter. However, theoretically, it is possible to calculate density from the refractive index using the Lorentz–Lorenz equation:

$$\frac{n^2 - 1}{n^2 + 2} = L \cdot \rho, \qquad (4)$$

where n represents the refractive index of the ice, ρ is its density, and L is the Lorentz–Lorenz coefficient (Guenther 2015).

In recent work, Domingo et al. (2021) showed that the Lorentz–Lorenz coefficient works for a set of molecules under astrophysical conditions, even for those that represent polar species. In the present work, the corresponding quotient $\frac{n^2-1}{n^2+2}$ versus density for CO has been plotted to look for the same relationship.

In Figure 5, the straight line represents the linear correlation between the quotient $\frac{n^2-1}{n^2+2}$ and density. Similar behavior is

Table 2
Experimental Values of the Lorentz–Lorenz Parameter Obtained for Each Temperature in This Work Compared with Other Values Present in the Literature

Temperature (K)	L (cm^3 g^{-1})	Author
13	0.206 ± 0.005	
14	0.213 ± 0.005	
15	0.213 ± 0.005	
16	0.214 ± 0.005	
17	0.214 ± 0.005	
18	0.210 ± 0.005	
19	0.212 ± 0.005	
20	0.213 ± 0.005	
21	0.210 ± 0.010	
22	0.215 ± 0.010	
23	0.208 ± 0.010	
24	0.216 ± 0.005	
26	0.214 ± 0.005	
28	0.214 ± 0.005	
…	Mean: 0.212 ± 0.006	This work
20	0.21	Roux et al. (1980)
35	0.21	Jiang et al. (1975)

obtained in the work of Domingo et al. (2021). The resulting straight line obtained in the present work lies in the central zone of the work of Domingo et al. (2021) (Figure 3, bottom), corresponding to polar molecules, confirming the trend they reported.

Applying the Lorentz–Lorenz formula, the constant L can be calculated and compared with the results achieved in other works. Table 2 compiles the L values obtained in this work for all the temperatures and the ones reported in the literature. As can be seen, there is a good agreement for all temperatures and for all authors leading to a value of $L = 0.212 \pm 0.006$ cm^3 g^{-1} that can be used to derive density from the refractive index at any temperature.

5. Conclusions

Carbon monoxide is one of the most abundant solid species in the frozen astrophysical scenarios. Under certain irradiation conditions, it is even a possible source of carbon dioxide, which is another relevant molecule. To understand the dynamics under astrophysical conditions of temperature, irradiation, and presence of other species, the study of several physical parameters of carbon monoxide has to be tackled.

This work focuses on studying density and refractive index at different temperatures of astrophysical interest. A set of deposition experiments at relevant temperatures has been performed. These results complement the scarce previous values reported in the literature. They help understand the behavior of this ice, obtain information from astronomical observations, and design and interpret irradiation experiments.

The values obtained for density and refractive index lie in the interval 0.85–0.89 g cm^{-3} and 1.28–1.30, respectively, presenting a similar profile with temperature (regardless of being two independent quantities), which confirms this trend as actual behavior.

An experimental relationship between density and refractive index has also been obtained, confirming the behavior reported previously by Domingo et al. (2021). The L factor of the Lorentz–Lorenz equation has also been obtained for all the temperatures. All the values are in good agreement and are similar to those reported in the literature. This result helps estimate values of density from the refractive index even for temperatures not selected in this work, regardless of whether it concerns an amorphous or crystalline structure.

ORCID iDs

Ramón Luna ⓘ https://orcid.org/0000-0001-8792-7578

References

Abplanalp, M. J., & Kaiser, R. I. 2019, PCCP, 21, 16949
Acharyya, K., Fuchs, G. W., Fraser, H. J., Van Dishoeck, E. F., & Linnartz, H. 2007, A&A, 466, 1005
Alsindi, W. Z., Gardner, D. O., Van Dishoeck, E. F., & Fraser, H. J. 2003, CPL, 378, 178
Beltrán, M. D., Molina, R. L., Aznar, M. Á. S., Moltó, C. S., & Verdú, C. M. 2015, Senso, 15, 25123
Bennett, C. J., Jamieson, C. S., & Kaiser, R. I. 2009, PCCP, 11, 4579
Bennett, C. J., Jamieson, C. S., & Kaiser, R. I. 2009, ApJS, 182, 1
Bennett, C. J., Jamieson, C. S., & Kaiser, R. I. 2010, PCCP, 12, 4032
Bennett, C. J., Hama, T., Kim, Y. S., Kawasaki, M., & Kaiser, R. I. 2011, ApJ, 727, 27
Bisschop, S. E., Fraser, H. J., Öberg, K. I., Van Dishoeck, E. F., & Schlemmer, S. 2006, A&A, 449, 1297
Bouilloud, M., Fray, N., Bénilan, Y., et al. 2015, MNRAS, 451, 2145
Brucato, J. R., Castorina, A. C., Palumbo, M. E., Satorre, M. A., & Strazzulla, G. 1997, P&SS, 45, 835
Brunetto, R., Caniglia, G., Baratta, G. A., & Palumbo, M. E. 2008, ApJ, 686, 1480
Cazaux, S., Martín-Doménech, R., Chen, Y. J., Muñoz Caro, G. M., & Cruz Diaz, G. A. 2017, ApJ, 849, 80
Chiar, J. E., Adamson, A. J., Kerr, T. H., & Whittet, D. C. B. 1994, ApJ, 426, 240
Ciaravella, A., Jiménez-Escobar, A., Muñoz Caro, G. M., et al. 2012, ApJ, 746, L1
Collings, M. P., Dever, J. W., Fraser, H. J., McCoustra, M. R. S., & Williams, D. A. 2003, ApJ, 583, 1058
Collings, M. P., Dever, J. W., Fraser, H. J., & McCoustra, M. R. S. 2003, Ap&SS, 285, 633
Cooke, I. R., Öberg, K. I., Fayolle, E. C., Peeler, Z., & Bergner, J. B. 2018, ApJ, 852, 75
Delsemme, A. H. 1983, JPhCh, 87, 4214
Domingo, M., Luna, R., Satorre, M. Á., Santonja, C., & Millán, C. 2021, ApJ, 906, 81
Ehrenfreund, P., Boogert, A. C. A., & Gerakines, P. A. 1996, A&A, 315, L341
Guenther, B. D. 2015, Modern Optics (Oxford: Oxford Univ. Press), doi:10.1093/acprof:oso/9780198738770.001.0001
Huang, C. H., Ciaravella, A., Cecchi-Pestellini, C., et al. 2020, ApJ, 889, 57
Hudson, R. L., & Moore, M. H. 1999, Icar, 140, 451
Jamieson, C. S., Mebel, A. M., & Kaiser, R. I. 2006, ApJS, 163, 184
Jiang, G. J., Person, W. B., & Brown, K. G. 1975, JChPh, 62, 1201
Kaiser, R. I., Maity, S., & Jones, B. M. 2014, PCCP, 16, 3399
Kerr, T. H., Adamson, A. J., & Whittet, D. C. B. 1993, MNRAS, 262, 1047
Kouchi, A. 1990, JCrGr, 99, 1220
Kouchi, A., Tsuge, M., Hama, T., et al. 2021, MNRAS, 505, 1530
Kouchi, A., Tsuge, M., Hama, T., et al. 2021, ApJ, 918, 45
Lacy, J., Baas, F., Allamandola, L. J., et al. 1984, ApJ, 276, 533
Lauck, T., Karssemeijer, L., Shulenberger, K., et al. 2015, ApJ, 801, 118
Lasne, J., Rosu-Finsen, A., Cassidy, A., McCoustra, M. R., & Field, D. 2015, PCCP, 17, 30177
Lellouch, E., de Bergh, C., Sicardy, B., Ferron, S., & Käufl, H. U. 2010, A&A, 512, L8
Lin, M. Y., Huang, T. P., Wu, P. Z., Chin, C. H., & Wu, Y. J. 2019, ApJ, 880, 132
Loeffler, M. J., Baratta, G. A., Palumbo, M. E., Strazzulla, G., & Baragiola, R. A. 2005, A&A, 435, 587
Luna, R., Satorre, M. Á., Santonja, C., & Domingo, M. 2014, A&A, 566, A27
Maity, S., Kaiser, R. I., & Jones, B. M. 2014, ApJ, 789, 36

Martín-Doménech, R., Muñoz Caro, G. M., Bueno, J., & Goesmann, F. 2014, A&A, 564, A8

Merlin, F. 2015, A&A, 582, A39

Mispelaer, F., Theulé, P., Aouididi, H., et al. 2013, A&A, 555, A13

Muñoz Caro, G. M., Chen, Y. J., Aparicio, S., et al. 2016, A&A, 589, A19

Öberg, K. I., van Broekhuizen, F., Fraser, H. J., et al. 2005, ApJ, 621, L33

Owen, T. C., Roush, T. L., Cruikshank, D. P., et al. 1993, Sci, 261, 745

Palumbo, M. E., Baratta, G. A., Collings, M. P., & McCoustra, M. R. S. 2006, PCCP, 8, 279

Penteado, E. M., Boogert, A. C. A., Pontoppidan, K. M., et al. 2015, MNRAS, 454, 531

Pipes, J. G., Roux, J. A., Smith, A. M., & Scott, H. E. 1978, AIAAJ, 16, 984

Polanyi, M., & Wigner, E. 1925, ZPhy, 33, 429

Quirico, E., & Schmitt, B. 1997, Icar, 128, 181

Roux, J. A., Wood, B. E., Smith, A. M., & Plyler, R. R. 1980, Arnold Engineering Development Center Int. Rep., Final Rep, AEDC-TR-79, Arnold Air Force Station

Satorre, M. A., Palumbo, M. E., & Strazzulla, G. 2000, Ap&SS, 274, 643

Satorre, M. Á., Domingo, M., Millán, C., et al. 2008, P&SS, 56, 1748

Satorre, M. Á., Leliwa-Kopystynski, J., Santonja, C., & Luna, R. 2013, Icar, 225, 703

Satorre, M. Á., Millán, C., Molpeceres, G., et al. 2017, Icar, 296, 179

Schmidt, F., Swiderek, P., & Bredehöft, J. H. 2019, ESC, 3, 1974

Schou, J., & Pedrys, R. 2001, JGR, 106, 33309

Seperuelo-Duarte, E., Domaracka, A., Boduch, P., et al. 2010, A&A, 512, A71

Takano, Y., Ushio, K., Kaneko, T., Kobayashi, K., & Hashimoto, H. 2003, Chem. Lett., 32, 612

Tegler, S. C., Stufflebeam, T. D., Grundy, W. M., et al. 2019, ApJ, 158, 17

Turner, A. M., Bergantini, A., Koutsogiannis, A. S., et al. 2021, ApJ, 916, 74

van Dishoeck, E. F., & Black, J. H. 1988, ApJ, 334, 771

Whittet, D. C. B., Adamson, A. J., Duley, W. W., Geballe, T. R., & McFadzean, A. D. 1989, MNRAS, 241, 707

Wood, B. E., & Roux, J. A. 1982, JOSA, 72, 720

Zamirri, L., Casassa, S., Rimola, A., et al. 2018, MNRAS, 480, 1427